

Letter

I-mode in non-deuterium plasmas in ASDEX Upgrade

N. Bonanomi^{1,*} , C. Angioni¹ , D. Silvagni^{1,2} , T. Happel¹ , U. Plank¹, L. Gil³ , P.A. Schneider¹ , T. Puetterich¹ , the EUROfusion MST1 Team^a and the ASDEX Upgrade Team^b

¹ Max Planck Institute for Plasma Physics, Boltzmannstr. 2, 85748 Garching, Germany

² Physik-Department E28, Technische Universität München, James-Franck-Str. 1, 85748 Garching, Germany

³ Instituto de Plasmas e Fusão Nuclear, Universidade Lisboa, PT, Portugal

E-mail: nicola.bonanomi@ipp.mpg.de

Received 13 January 2021, revised 11 February 2021

Accepted for publication 4 March 2021

Published 12 April 2021



CrossMark

Abstract

The I-mode confinement regime in non-deuterium plasmas has been investigated in the ASDEX Upgrade tokamak. We report the first experimental observations on the existence and the main characteristics of this regime in hydrogen and helium plasmas and compare them with deuterium I-modes. Hydrogen features a higher power threshold to enter I-mode and a higher electron edge pressure at the L- to I-mode transition with respect to deuterium. Furthermore, all the hydrogen I-modes obtained exhibit pedestal relaxation events (PRE). The I-mode power window in hydrogen is found to be 2–3 times larger than in deuterium. This property allows a better characterization of PRE and to differentiate them from type-III ELMs. Helium I-modes feature properties which are similar to those of deuterium I-modes. The analysis on the minimum of the edge radial electric field E_r shows a correlation between the E_r minimum, the net input power and the ion diamagnetic term in the ion radial force balance. Indications of the dominant role of the edge ion temperature in the evolution of the radial electric field with increasing input power are also reported.

Keywords: ASDEX Upgrade, I-mode, isotope mass, turbulent transport, ELM-free regimes

(Some figures may appear in colour only in the online journal)

1. Introduction

The I-mode regime is characterized by having an improved edge energy confinement while keeping density profiles

typical of the L-mode regime [1–4]. This allows for a high core plasma pressure without reaching the ideal peeling-ballooning instability limit in the pedestal region and avoiding in this way the presence of type-I ELMs [5–7]. Nevertheless, when the pedestal pressure is high enough (typically close to the transition to H-mode), pedestal relaxation events (PRE) [8] and intermittent turbulence bursts [9] can appear. These are losses of energy and particles from the plasma edge that lead to smaller relative energy loss ($\approx 1\%$) compared to type-I ELMs. PREs have been observed in ASDEX Upgrade [8] as well as in Alcator C-Mod [6]. The behavior of the I-mode edge confinement is most likely related to the properties of the edge tur-

* Author to whom any correspondence should be addressed.

^a See Labit *et al* 2019 (<https://doi.org/10.1088/1741-4326/ab2211>) for the EUROfusion MST1 Team.

^b See Meyer *et al* 2019 (<https://doi.org/10.1088/1741-4326/ab18b8>) for the ASDEX Upgrade Team.



Original content from this work may be used under the terms of the [Creative Commons Attribution 3.0 licence](https://creativecommons.org/licenses/by/3.0/). Any further distribution of this work must maintain attribution to the author(s) and the title of the work, journal citation and DOI.

bulent transport in this regime. The appearance of the weakly coherent modes (WCM) [2, 10] is usually observed in I-mode and it is believed to be associated with the properties of the I-mode edge turbulence [10–12]. However, in C-Mod and in ASDEX Upgrade, the WCM have been observed also in the L-mode phase [13, 14] and, in DIII-D, I-modes with no clear indications of WCM have been observed [4]. These characteristics of the I-mode make it a type-I-ELM-free improved confinement regime possibly relevant for the operations of a future reactor, but also a source of precious information for the understanding of the edge turbulence and the different regimes of turbulence stabilization. An important aspect of the plasma edge turbulence is its dependence on the main ion mass [15]. A strong dependence of the plasma confinement on the main ion mass is a general feature of tokamak plasmas [16–19], largely determined by properties of the edge. Furthermore, a future reactor will operate in a mixed isotope plasma of deuterium and tritium. In order to develop reliable ELM-free scenarios and in order to extrapolate these scenarios to future reactors it is then important to understand what controls the edge turbulence and how this is influenced by the main ion mass. To the knowledge of the authors, no ELM-free high-confinement regime in non-deuterium plasmas have been observed so far in tokamaks. In the effort to fill this gap, a series of experiments has been started recently in the ASDEX Upgrade (AUG) tokamak. We report here on the main results on I-modes obtained in hydrogen (H) and helium (He) plasmas and compare their characteristics with those of deuterium (D) I-modes. This paper is organized as follows: in section 2 the experimental settings and parameters are reported, in section 3 the main results in hydrogen and helium I-modes are reported while in section 4 a comparison between H, D and He is given. In section 5 the conclusions are drawn.

2. Experimental settings

The experiments reported here were all performed in the ASDEX Upgrade tokamak (major radius $R_0 = 1.65$ m, minor radius $a = 0.5$ m) with a full tungsten wall. All the plasmas are in the upper single null (USN) configuration in order for the ion ∇B -drift to point away from the active X-point. This allows us to also have a higher H-mode power threshold, important for the development of the I-mode [1, 7, 20]. The plasma current and the toroidal magnetic field are $I_p = 1$ MA and $B_T = -2.5$ T with the safety factor at the 95% of the toroidal flux $q_{95} \approx 4$. The line-averaged core density was kept around $\bar{n}_e \approx 6 \times 10^{19} \text{ m}^{-3}$. Slow scans in the electron cyclotron resonance heating (ECRH) power and in the neutral beam injector (NBI) heating power were performed in order to observe the plasma evolution from L- to I-mode and from I- to H-mode. Regarding the NBI heating, hydrogen NBI was used in hydrogen plasmas (allowing a hydrogen concentration $n_H/n_e \gtrsim 90\%$), while deuterium NBI was used in helium experiments, with a resulting He concentration of $n_{\text{He}}/n_e \sim 28\%–35\%$, meaning 60%–70% of the total ion charge. The net input power is defined as $P_{\text{net}} = P_{\text{NBI}} + P_{\text{ECRH}} + P_{\text{OHM}} - dW_{\text{MHD}}/dt$, where P_{NBI} is the NBI heating power, P_{ECRH} is the ECRH power, P_{OHM} is the ohmic power and W_{MHD} is the

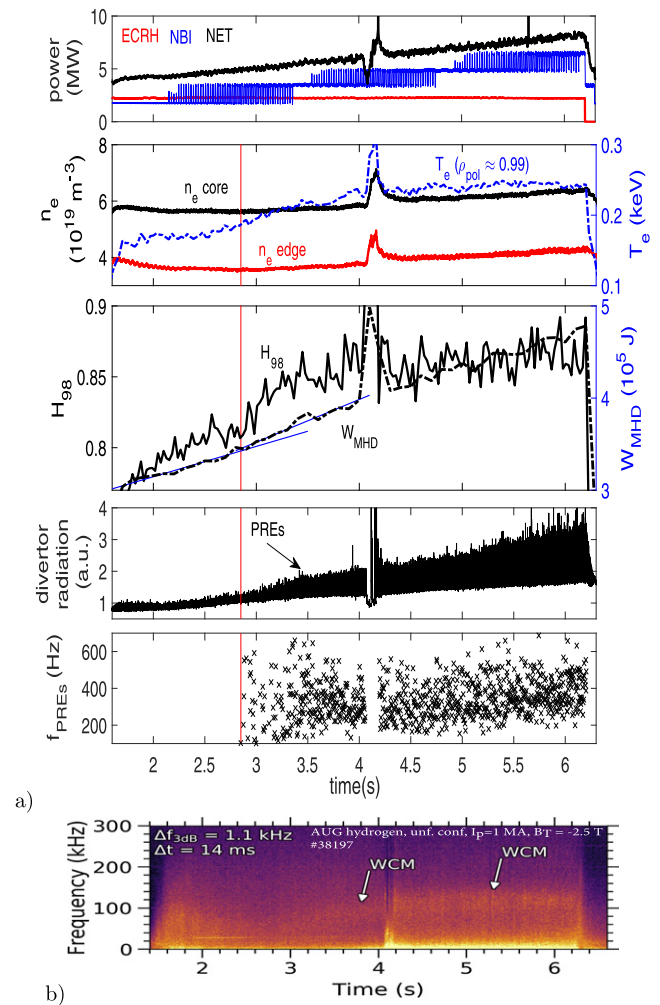


Figure 1. (a) Time traces of the input heating power, line averaged core and edge densities and T_e close to the separatrix, H_{98} factor and stored energy, radiation at the outer upper divertor and PRE frequencies. The H_{98} factor during the H-mode phase reaches the value of $H_{98} = 1.2$. Linear fits of the plasma stored energy are also plotted (blue lines) to help to visualize the change in slope of W_{MHD} after the L–I transition. (b) Density fluctuations spectrogram in the plasma edge showing the evolution of the WCM. The data is taken from the AUG hydrogen shot #38197 with upper single null configuration, $I_p = 1$ MA and $B_T = -2.5$ T. After $t \approx 2.8$ s the raise of the edge temperature (while the density stays at the same level), the change in slope of the plasma stored energy evolution, the appearance of PREs and the appearance of the WCMs indicate that the plasma enters into I-mode.

MHD plasma stored energy. In order to compute the plasma thermal stored energies, the fast particle energy contents from NBI have been computed using RABBIT [21] through a procedure newly developed at AUG [22]. The electron temperature (T_e) profiles are measured using the electron cyclotron emission and the core and edge Thomson scattering diagnostics. The ion temperature (T_i) profiles are measured using the core and edge charge exchange diagnostics while the electron density profiles (n_e) are measured using the Thomson scattering data, the interferometer signals and the fits performed using the integrated data analysis Bayesian approach [23]. A new diagnostic based on the active spectroscopy of singly ionized helium, which measures the radial electric field E_r around

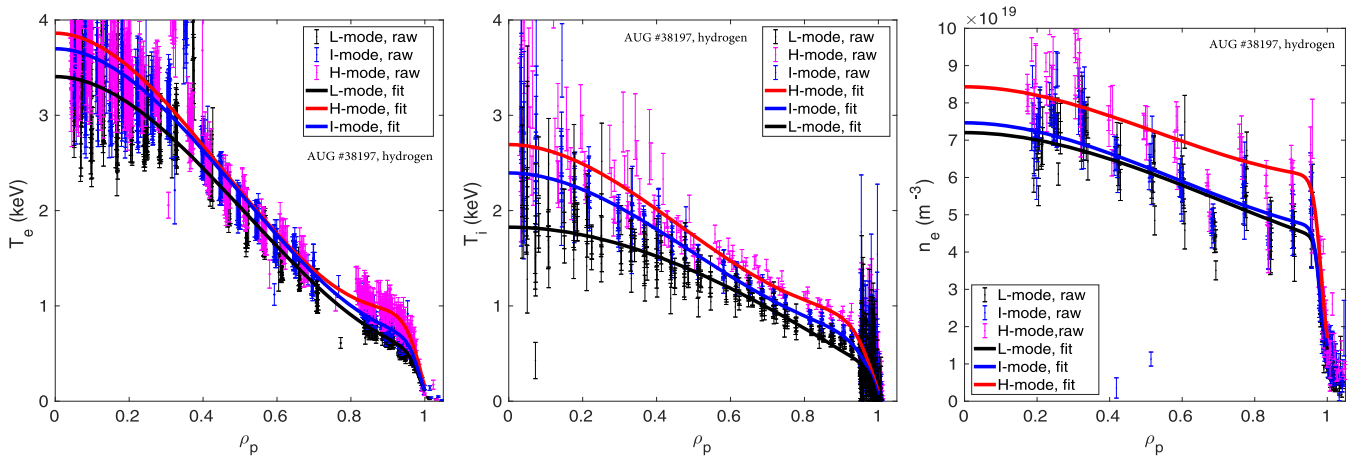


Figure 2. Radial profiles of the electron temperature T_e , the ion temperature T_i and the electron density n_e during the L-, I- and H-mode phases for hydrogen shot #38 197. The time intervals are $2.4 \leq t \leq 2.8$ s for L-mode, $3.6 \leq t \leq 4.0$ s for I-mode and $4.08 \leq t \leq 4.16$ s for H-mode.

the separatrix [24], has been used to study the evolution of the E_r minimum in the confined region. In order to observe the presence of the WCM density fluctuations measurements were performed in the edge region using reflectometry. The radiation at the upper outer divertor from diode bolometers is used to study the PRE. Other quantities shown in this work are the H_{98} factor [25], the plasma confinement time in seconds defined as $\tau_E = W_{\text{MHD}}/P_{\text{net}}$, and the normalized gradients $R/L_{T_{i,e}} = -R_0 \cdot \nabla_r T_{i,e}/T_{i,e}$ and R/L_{n_e} calculated using the plasma minor radius $r = (R_{\text{out}} - R_{\text{in}})/2$, R_{out} and R_{in} being the outer and inner major radius of the plasma flux surfaces, for the gradients. The poloidal radius $\rho_p = \sqrt{\Psi/\Psi_{\text{max}}}$, where Ψ is the poloidal flux, is used in most of the plots.

3. I-mode in hydrogen and helium

In figure 1(a) we report the time evolution of the heating power, of the line-averaged core and edge densities, of the electron temperature close to the separatrix, of the H_{98} factor, of the plasma stored energy W_{MHD} , of the radiation at the upper outer divertor and of the PRE frequencies for hydrogen shot #38 197. The time evolution of the density fluctuations spectrogram in the plasma edge from the same discharge is shown in figure 1(b). Around $t = 2.8$ s the transition from L- to I-mode occurs at $\bar{n}_e = 5.7 \times 10^{19} \text{ m}^{-3}$ and $P_{\text{NET}} = 4.8$ MW (in D with similar parameters the L–I threshold is around $P_{\text{NET}} = 3.8$ MW). At the same time the WCM starts to develop and PRE appear (figure 1(a)). The plasma enters into H-mode around $t = 4.07$ s and around $t = 4.16$ s it returns into I-mode with increased density and stays in I-mode until the end of the discharge. This behavior can be explained as a consequence of the change in density. When the plasma enters H-mode, the density increases suddenly, moving the H-mode power threshold to higher values, while the heating power increases too slowly to follow this change. As a consequence the plasma goes back to I-mode with increased density and more power is needed to re-enter into H-mode. A similar behavior has been observed also in shot #38 196. In that case, a transition into H-mode occurred at $\bar{n}_e \approx 5.8 \times 10^{19} \text{ m}^{-3}$ and

$P_{\text{net}} \approx 5.48$ MW, the plasma went back into I-mode with $\bar{n}_e \approx 6.36 \times 10^{19} \text{ m}^{-3}$ and, because a faster NBI heating power scan was applied, it re-entered H-mode at $P_{\text{net}} \approx 6.9$ MW before the end of the discharge. In shot #38 197, before the I- to H-mode transition, the net input power peaks around $P_{\text{net}} = 6.2$ MW. This indicates that the operational power window for the I-mode in hydrogen is larger with respect to the deuterium one (typically $\lesssim 1$ MW). In shot #38 182, at rather constant density, the I-mode phase is in the range $4 \lesssim P_{\text{NET}} \lesssim 7.2$ MW, so a power operational window of 3 MW is possible for I-mode in hydrogen. This, in combination with the observation that all the I-modes obtained in hydrogen exhibit PRE from the beginning, made it possible to study PRE in more detail. It is found that PRE amplitudes increase with increasing input power and that their frequencies do not decrease, or slightly increase, with heating power (figure 1(a)). These characteristics differentiate PRE from type-III ELMs, for which the frequencies decrease with increasing input power [26].

The plasma kinetic profiles in the L-, I- and H-mode phases of shot #38 197 are plotted in figure 2. The formation of an edge pedestal in T_i and T_e , but not in n_e , during the I-mode phase is visible, while in H-mode a pedestal also in the density appears. The confinement in the I-mode phase is not strongly increased with respect to the L-mode phase in hydrogen. This can be seen looking at the H_{98} factor (figure 1(a)), that increases only from 0.82 to 0.85. This small increase can be related to the fact that, at the high input power needed in hydrogen to enter in I-mode, the electron pedestal pressure before the L–I transition is almost at the same level of the one in I-mode and also the H_{98} factor is already pretty high in the L-mode phase. In figure 3(a) the time evolution of the edge E_r minimum and of T_i, T_e, n_e and $R/L_{T_i}, R/L_{T_e}, R/L_{n_e}$, measured around $\rho_{\text{pol}} = 0.98$, is shown for shot #38 197. A development of the E_r well, indicated by the decrease of the E_r minimum, is visible only after the L–I transition, consistent with measurements in D [7]. T_i and R/L_{T_i} feature the strongest evolution after the L–I transition, with a jump in T_i and an evolution with power of R/L_{T_i} . Also T_e evolves with power, while

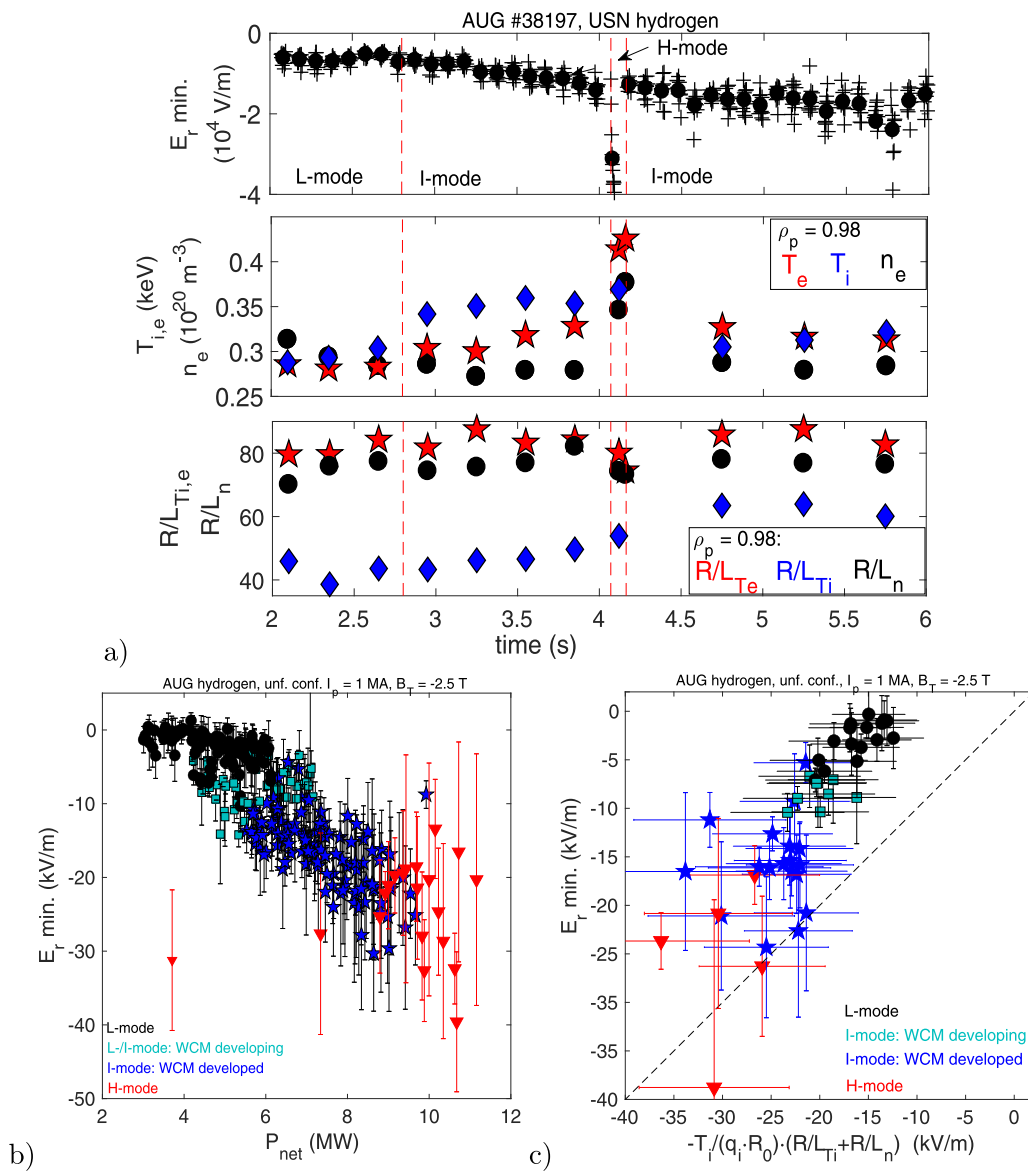


Figure 3. (a) Time traces of the edge radial electric field minimum, of T_e , T_i , n_e measured at $\rho_{\text{pol}} \approx 0.98$ and of R/L_{T_e} , R/L_{T_i} , R/L_n measured at $\rho_{\text{pol}} \approx 0.98$ of hydrogen shot #38 197. (b) Edge radial electric field minimum as a function of the net input power for all the hydrogen shots of the same session. (c) Edge radial electric field minimum as a function of $-T_i/(q_i \cdot R_0) \cdot (R/L_{T_i} + R/L_n)$, i.e. the ion diamagnetic term from the ion radial force balance equation, averaged on $0.97 \leq \rho_{\text{pol}} \leq 0.98$.

n_e , except during the H-mode phase, does not exhibit strong variations. R/L_{T_e} and R/L_n do not evolve much during the whole discharge. These behaviors are common to all the hydrogen discharges obtained in this study and indicate a strong correlation between the evolution of the edge E_r and the evolution of T_i and R/L_{T_i} . In figures 3(b) and (c) we show the evolution of the edge E_r minimum as a function of the net input power and as a function of $T_i/n_i/R \cdot (R/L_{T_i} + R/L_n)$. This quantity represents the diamagnetic term in the ion radial force balance equation and is measured for all the hydrogen shots averaging on $0.97 \leq \rho_p \leq 0.98$ and using n_e as a proxy for the ion density. A correlation of the edge E_r minimum with the net input power and with the ion diamagnetic term is visible, further confirming that the ion temperature evolution with input power determines the evolution of E_r and possibly also

the L–I and I–H transitions. These observations are consistent with past observations on this aspect [27, 28]. An offset, stronger in L-mode and reduced going towards the H-mode, is present between the measured values of the E_r minimum and the values calculated using the ion diamagnetic term. This can indicate that at low values of the diamagnetic term, typical of L-modes where the ion temperature is low and with low values of R/L_{T_i} , the $\mathbf{v} \times \mathbf{B}$ term in the radial force balance could have, at least in this unfavorable drift configuration, a bigger impact. This observation motivates future studies on this aspect, also including dedicated comparisons with D plasmas.

Regarding helium, we report here the main results from the observation of a brief ($5.25 \lesssim t \lesssim 5.32$ s) I-mode phase observed, where WCM are evolving (figure 4(b)) and both phases with and without PRE are present (figure 4(a)). The

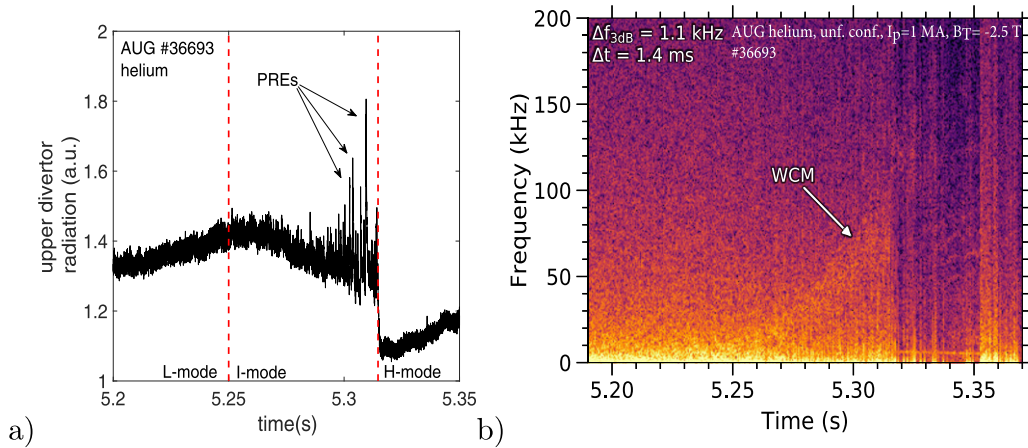


Figure 4. (a) Time evolution of the radiation at the upper outer divertor. (b) Spectrogram of the density fluctuations from reflectometry. The data are taken from helium AUG shot #36 693.

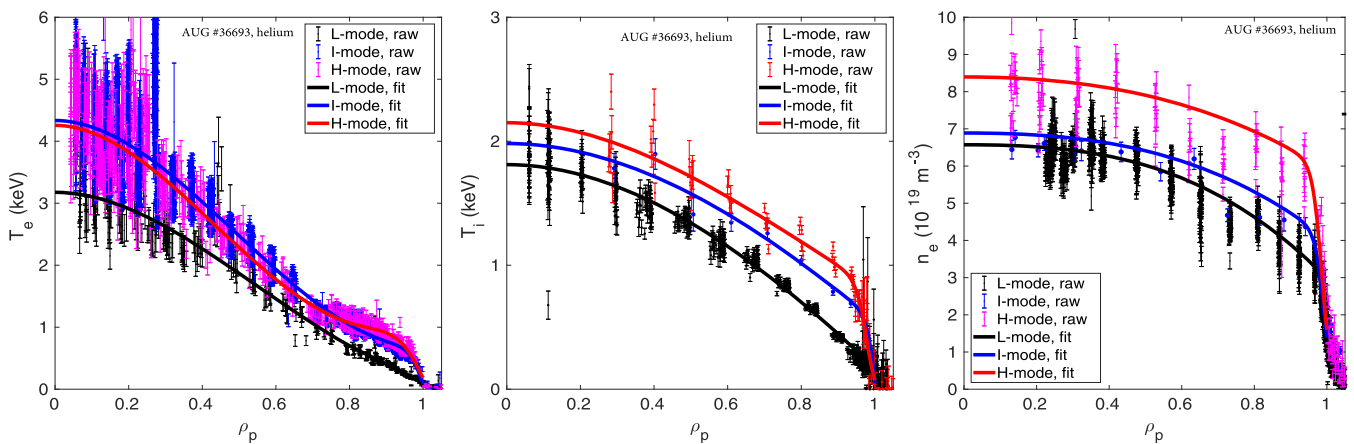


Figure 5. Radial profiles of the electron temperature T_e , the ion temperature T_i and the electron density n_e during the L-, I- and H-mode phases for helium shot #36 693. The time intervals are $4.5 \leq t \leq 5$ s for L-mode, $5.27 \leq t \leq 5.315$ s for I-mode and $5.35 \leq t \leq 5.5$ s for H-mode.

global plasma parameters (such as B_T , I_p , n_e and q_{95}) were similar to the hydrogen case but the I-mode was observed during the last phase of the discharge when the plasma current decreased to $I_p = 0.85$ MA. In this case the L- to I-mode power threshold at $\bar{n}_e \approx 6 \times 10^{19} \text{ m}^{-3}$ is around $P_{\text{NET}} = 3.8$ MW, and the H_{98} factor strongly increases from 0.6 in L-mode to 0.94 in I-mode. These numbers compare well with those in D plasmas with similar plasma parameters. Similar to D is also the evolution of the plasma profiles, with a strong evolution of the edge T_i and T_e from L- to I-mode (figure 5). Starting from this first observation, more experiments are clearly required in the future to allow a more complete characterization of the properties of the I-mode in He plasmas.

4. Comparison between H, D and He I-mode properties

In figure 6 the L-, I- and H-mode phases in the (T_e^{95}, n_e^{95}) and (T_i^{95}, n_e^{95}) spaces (with T_e, T_i, n_e measured at $\rho_{\text{pol}} = 0.95$) for hydrogen, deuterium and helium are shown. In D plasmas the L- to I-mode transition occurs around the isobar line

$p_e^{95} = 2$ kPa and PRE start close to the I- to H-mode transition, at values around the isobar line $p_{e,95} = 4$ kPa. The two points available for helium, one with and one without PRE, lie within these values and compare well with deuterium. In hydrogen, the transition into I-mode occurs at electron pressures around the isobar line $p_{95} = 4$ kPa. This corresponds to the region where PRE are present in deuterium and indeed all the hydrogen I-modes observed feature PRE. Also the transition into H-mode is shifted to higher values of p_{95} in hydrogen. Similar conclusions are obtained if T_i^{95} is used instead of T_e^{95} for hydrogen and helium (figure 6). As already documented from the profiles shown in figure 5, a strong jump in the edge ion temperature occurs after the L- to I-mode transition in helium, while in hydrogen the change in edge temperatures is less strong.

In figure 7 three plots related to the plasma confinement are shown: the net input power as a function of the electron pressure measured at $\rho_{\text{pol}} = 0.95$ (left), the H_{98} factor as a function of p_e^{95} (center) and the energy confinement time in seconds, τ_E , as a function of P_{net} (right). Much more heating power is needed in hydrogen to obtain the same

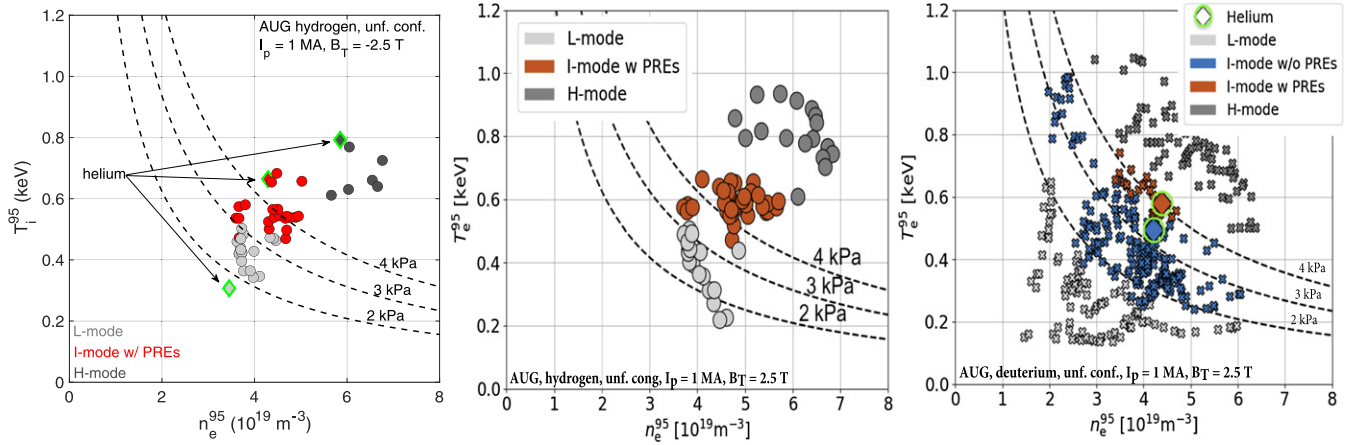


Figure 6. Operational space in $(n_e, T_e)_{95}$, i.e. measured at $\rho_p = 0.95$, for L-, I- and H-mode in hydrogen (left) and operational space in $(n_e, T_e)_{95}$ for L-, I- and H-mode in hydrogen (center) and deuterium and helium (right). All the points are with $I_p = 1 \text{ MA}$, $B_T = -2.5 \text{ T}$, $q_{95} = 4$.

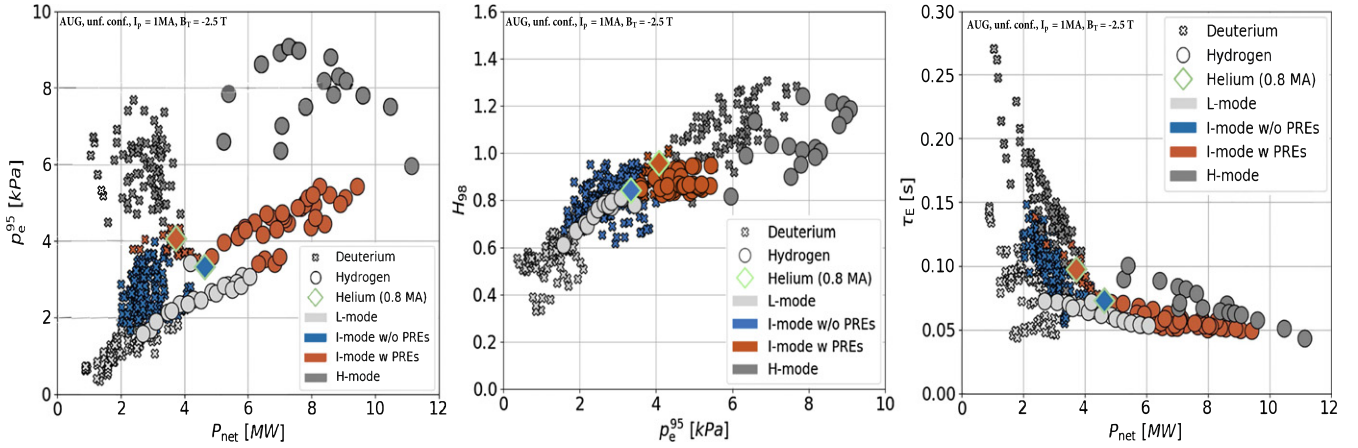


Figure 7. Electron pressure measured at $\rho_p = 0.95$ as a function of the input heating power (left). H_{98} factor as a function of the electron pressure at $\rho_p = 0.95$ (center). Confinement time in seconds as a function of the net input power (right).

deuterium electron pedestal pressure. As a consequence the plasma confinement times are lower in hydrogen, the strong degradation in τ_E in hydrogen with increasing P_{net} indicating that hydrogen is much more resilient to a change in plasma stored energy with input power. Similar H_{98} factors can be obtained between hydrogen and deuterium but in hydrogen higher values are obtained in the L-mode phase, as the temperature raises with the high input power required to enter I-mode and H-mode in hydrogen. This determines a weak improvement in the H_{98} factor between the L-mode and the I-mode phases in hydrogen. Generally, the H_{98} factor does not increase as much as in deuterium in the hydrogen I-modes phases observed in this work, and it raises again only when the plasma enters H-mode. These observations indicate that the confinement in hydrogen is worse than in deuterium plasmas and the edge region is playing an important role in this. All these observations can be related to the higher edge turbulence level of hydrogen [15, 29]. Much more power is needed to evolve R/L_{Ti} , and the edge E_r , in hydrogen [30]. At the same

time the edge temperatures, especially the electron temperature, evolve with the strong heating power and reach higher values in hydrogen L-mode compared to deuterium at the transition but do not exceed those in deuterium once in I-mode or H-mode. This causes a less pronounced increase in confinement from L- to I-mode in hydrogen and lower values of quantities that depend on the input power such as H_{98} and τ_E .

5. Conclusions

The existence of I-modes in hydrogen (H) and helium (He) has been proven for the first time in plasmas obtained in the ASDEX Upgrade tokamak and their main characteristics have been reported. Higher input power is needed in hydrogen to enter into I-mode and to obtain similar plasma profiles with respect to deuterium. Furthermore, H plasmas enter I-mode at a higher edge electron pressure than in D plasmas and all

the observed hydrogen I-modes feature PRE. The operational power window of 3 MW in H is larger than in D, where it is below 1 MW at AUG. These characteristics allowed us to study the PRE evolution in more detail. Their frequency is observed to not decrease with increasing input power while their amplitudes increase with increasing input power. These properties differentiate them from other edge events such as type-I and type-III ELMs. Hydrogen generally features a lower confinement than deuterium and also the confinement improvement from L- to I-mode is more limited in hydrogen plasmas. This can be related to the higher edge L-mode turbulence with lower isotope mass and to the much higher input power, and gas puffing, needed to obtain similar plasma pressures than in D plasmas. Regarding He, only a short I-mode phase was obtained featuring properties similar to D I-modes with similar plasma parameters. Both phases with and without PRE were observed in helium, which occur at the same isobars as in deuterium. A study on the behavior of the minimum of the edge radial electric field shows a correlation of the E_r minimum with the net input power and of the E_r minimum with the diamagnetic term of the main ions in the radial force balance. As the density and R/L_n were found to not evolve much with input power (although n_e evolves during the H-mode phases), these observations point to a central role in $T_i \cdot R/L_{Ti}$ in determining E_r . A deviation of the E_r minimum from the diamagnetic term is observed in the L-mode phases, indicating that in these plasma conditions, the plasma rotation might play an increased role in the determination of E_r . These I-mode results in non-deuterium plasmas deliver a fundamental base for future studies and can help to improve our understanding of edge turbulence properties as well as of the WCM, which can be associated with particular edge turbulence properties of the I-mode regime.

Acknowledgment

The authors are grateful to D. Fajardo, G. Tardini and M. Weiland for the computation of the beam ion energy content with the RABBIT code. This work has been carried out within the framework of the EUROfusion Consortium and has received funding from the EURATOM research and training programme 2014–2018 and 2019–2020 under Grant Agreement No. 633053. The views and opinions expressed herein do not necessarily reflect those of the European Commission.

ORCID iDs

N. Bonanomi  <https://orcid.org/0000-0003-4344-3330>
 C. Angioni  <https://orcid.org/0000-0003-0270-9630>
 D. Silvagni  <https://orcid.org/0000-0003-2103-3592>
 T. Happel  <https://orcid.org/0000-0003-4364-9363>
 L. Gil  <https://orcid.org/0000-0002-9970-2154>
 P.A. Schneider  <https://orcid.org/0000-0001-7257-3412>
 T. Puetterich  <https://orcid.org/0000-0002-8487-4973>

References

- [1] Ryter F. et al 1998 *Plasma Phys. Control. Fusion* **40** 725
- [2] Whyte D.G. et al 2010 *Nucl. Fusion* **50** 105005
- [3] Liu Y.J. et al 2020 *Nucl. Fusion* **60** 082003
- [4] Marinoni A. et al 2015 *Nucl. Fusion* **55** 093019
- [5] Hughes J.W. et al 2013 *Nucl. Fusion* **53** 043016
- [6] Walk J.R. et al 2014 *Phys. Plasmas* **21** 056103
- [7] Happel T. et al 2017 *Plasma Phys. Control. Fusion* **59** 014004
- [8] Silvagni D. et al 2020 *Nucl. Fusion* **60** 126028
- [9] Happel T. et al 2016 *Nucl. Fusion* **56** 064004
- [10] Hubbard A.E. et al 2011 *Phys. Plasmas* **18** 056115
- [11] Manz P. et al 2015 *Nucl. Fusion* **55** 083004
- [12] Manz P., Happel T., Stroth U., Eich T. and Silvagni D. 2020 *Nucl. Fusion* **60** 096011
- [13] Happel T. et al 2019 *Nucl. Mater. Energy* **18** 159–65
- [14] Bielajew R. et al Electron temperature fluctuation measurements in the I-mode pedestal ASDEX Upgrade 62nd Annual Meeting of the APS Division of Plasma Physics (9-11-2020–13-11-2020) Poster NP15.00001
- [15] Bonanomi N., Angioni C., Crandall P.C., Di Siena A., Maggi C.F. and Schneider P.A. 2019 *Nucl. Fusion* **59** 126025
- [16] Bessenrodt-Weberpals M. et al 1993 *Nucl. Fusion* **33** 1205
- [17] Barnes C.W. et al 1996 *Phys. Plasmas* **3** 4521
- [18] Maggi C.F. et al 2018 *Plasma Phys. Control. Fusion* **60** 014045
- [19] Schneider P.A. et al 2017 *Nucl. Fusion* **57** 066003
- [20] Ryter F. et al 2017 *Nucl. Fusion* **57** 016004
- [21] Weiland M., Bilato R., Dux R., Geiger B., Lebschy A., Felici F., Fischer R., Rittich D. and van Zeeland M. 2018 *Nucl. Fusion* **58** 082032
- [22] Tardini G. et al 2021 *Nucl. Fusion* **61** 036030
- [23] Fischer R. et al 2010 *Fusion Sci. Technol.* **58** 675–84
- [24] Plank Ulrike. et al 2020 Private communication
- [25] ITER Physics Expert Group on Confinement and Transport et al 1999 *Nucl. Fusion* **39** 2175–249
- [26] Zohm H. 1996 *Plasma Phys. Control. Fusion* **38** 105
- [27] Ryter F., Barrera Orte L., Kurzan B., McDermott R.M., Tardini G., Viezzer E., Bernert M. and Fischer R. 2014 *Nucl. Fusion* **54** 083003
- [28] Schmidtmayr M. et al 2018 *Nucl. Fusion* **58** 056003
- [29] Belli E. et al 2020 *Phys. Rev. Lett.* **125** 015001
- [30] Bonanomi N. et al 2020 *Plasma Phys.* private communication